TISSUE ENGINEERING: Part A
Volume 20, Numbers 13 and 14, 2014

DOI: 10.1089/ten.tea.2013.0513

Three-Dimensional Printing of rhBMP-2-Loaded Scaffolds with Long-Term Delivery for Enhanced Bone Regeneration in a Rabbit Diaphyseal Defect

Jin-Hyung Shim, PhD,[1,*] Se Eun Kim, DVM, PhD,[2,*] Ju Young Park, MS,[3] Joydip Kundu, PhD,[4] Sung Won Kim, MD, PhD,[5] Seong Soo Kang, DVM, PhD,[2] and Dong-Woo Cho, PhD[4]

In this study, recombinant human bone morphogenetic protein-2 (rhBMP-2) delivery system with slow mode was successfully developed in three-dimensional (3D) printing-based polycaprolactone (PCL)/poly(lactic-co-glycolic acid) (PLGA) scaffolds for bone formation of critical-sized rabbit segmental diaphyseal defect. To control the delivery of the rhBMP-2, collagen (for long-term delivery up to 28 days) and gelatin (for shor-term delivery within a week) solutions encapsulating rhBMP-2 were dispensed into a hollow cylinderical type of PCL/PLGA scaffold. An effective dose of 5μg/mL was determined by measuring the *alkaline phosphatase* and *osteocalcin* gene expression levels of human nasal inferior turbinate-derived mesenchymal stromal cells (hTMSCs) seeded on the PCL/PLGA/collagen scaffold in vitro. However, it was found that a burst release of rhBMP-2 from the PCL/PLGA/gelatin scaffold did not induce the osteogenic differentiation of hTMSCs in vitro at an equivalent dose. In the *in vivo* animal experiements, microcomputed tomography and histological analyses confirmed that PCL/PLGA/collagen/rhBMP-2 scaffolds (long-term delivery mode) showed the best bone healing quality at both weeks 4 and 8 after implantation without inflammatory response. On the other hand, a large number of macrophages indicating severe inflammation provoked by burst release of rhBMP-2 were observed in the vicinity of PCL/PLGA/gelatin/rhBMP-2 (short-term delivery mode) at week 4.

Introduction

Repair of critical-sized bone defects caused by congenital deformation, trauma, and tumor ablation is still a challenge in orthopedics.[1,2] In these cases, the Ilizarov bone transport technique,[3] autologous bone,[4] and artificial bone grafts[5] are mainly used to restore the critical-sized bone defects. However, each method has drawbacks. A critical problem of the Ilizarov technique is the patient's inconvenience from the external fixation.[6] On the other hand, significant donor site morbidity is always mentioned as a main drawback of autologous bone grafting to be used in critical-sized defects.[7] Nondegradability is a critical limitation preventing artificial bone grafts consisting of metal or ceramic from being a a gold standard in orthopedics.[8] Thus, tissue engineering has been considered to be a promising therapeutic approach for reconstructing an extensive bone loss.

In tissue engineering, a biocompatible three-dimensional (3D) porous scaffold is required to regenerate and repair tissue loss.[9] Moreover, its pores should be fully interconnected. Adequate mechanical property is an essential requirement for bone tissue regeneration. In addition, the customized scaffold is particularly required to be used in bone regeneration of critical-sized defects having complex geometry. In light of this, 3D printing technology enabling the fabrication of customized 3D scaffolds that are geometrically complex using a layer-by-layer process has been widely utilized as an effective technology in tissue engineering.[10–12] Indeed, a commercially available 3D polycaprolactone (PCL) scaffold (Osteopore International Pte) approved by the Food and Drug Administration (FDA) for bone tissue engineering has been developed based on fused deposition modeling, a type of 3D printing technology.[13] In addition, 3D-printed cranial implants using polymethylmethacrylate (OXPEKK-IG OsteoFab; Oxford Performance Materials) was recently approved by the FDA for implantation in human skulls.[14] Three-dimensional printing-based scaffolds have demonstrated a remarkable potential for bone

[1]Department of Mechanical Engineering, Korea Polytechnic University, Siheung, South Korea.
[2]Department of Surgery, College of Veterinary Medicine, Chonnam National University, Gwangju, South Korea.
[3]Division of Integrative Biosciences and Biotechnology, Pohang University of Science and Technology (POSTECH), Kyungbuk, South Korea.
[4]Department of Mechanical Engineering, Pohang University of Science and Technology (POSTECH), Kyungbuk, South Korea.
[5]Department of Otolaryngology-Head and Neck Surgery, Seoul St. Mary's Hospital, College of Medicine, The Catholic University of Korea, Seoul, South Korea.
*These authors contributed equally to this work.

formation and healing.[15,16] Research interest in 3D printing-based scaffold is now focused on how to functionalize the scaffolds to accelerate the bone healing process.

Meanwhile, recombinant human bone morphogenetic protein-2 (rhBMP-2) is recognized as the most potent growth factor for bone formation and repair due to its powerful osteoinductive ability.[17] The rhBMP-2, which is clinically approved by the FDA, has been used for various clinical applications such as intervertebral spinal fusion,[18] open tibia fracture,[19] and dental bone graft.[20] Despite its efficacy, it has been reported that sustained and local delivery of rhBMP-2 using a suitable carrier is essentially required to accelerate bone healing.[21,22] Recently, a variety of sustained rhBMP-2 delivery systems based on 3D printing technology have been introduced.[23–25] Park *et al.* developed an solid freeform fabrication-based 3D scaffold consisting of poly (lactic-co-glycolic acid) (PLGA) grafted with hyaluronic acid, in which an intact BMP-2/poly (ethylence glycol) complex was encapsulated.[23] In addition, Lee *et al.* developed poly(propylene fumarate)/diethyl fumarate scaffolds embedded with rhBMP-2 delivering PLGA microspheres using a microstereolithography system.[24] Although new bone formation was enhanced by the rhBMP-2-loaded scaffolds, toxic organic solvent was used in both fabrication processes, which can be an obstacle for clinical applications due to the health risks associated with the residual organic solvent. On the other hand, it was reported that the 3D printing-based medical grade PCL-tricalcium phosphate scaffold filled with dried collagen was immersed into rhBMP-2 solution for a delivery system.[25] However, the dipping method could cause inconsistent loading quantity of rhBMP-2 in the scaffold and a waste of rhBMP-2 exceeding the amount necessary. To overcome these limitations, we developed a 3D printing-based rhBMP-2 delivering scaffold with only clinically relevent biomaterials and processes using a multi-head deposition system (MHDS). Notably, controllable delivery systems were simply implemented by dispensing collagen and gelatin solution into hollow cylindrical PCL/PLGA scaffolds. An effective *in vitro* rhBMP-2 dose was investigated by measuring the expression level of osteogenic gene markers of human nasal inferior turbinate-derived mesenchymal stromal cells (hTMSCs). Moreover, the effects of sustained and burst releases of rhBMP-2 on the formation of bone were studied by implanting the PCL/PLGA (group 1), PCL/PLGA/gelatin/rhBMP-2 (group 2), and PCL/PLGA/collagen/rhBMP-2 (group 3) scaffolds into a 20-mm segmental diaphyseal defect in a rabbit. At that time, customized 3D scaffold whose shape was the same as diaphyseal defect of rabbit was fabricated using 3D printing technology. Microcomputed tomography (μCT), histology, and immunohistochemical analyses were utilized to analyze the degree of bone formation and inflammatory response *in vivo*.

Materials and Methods

Fabrication of 3D printing-based PCL/PLGA scaffolds encapsulating intact rhBMP-2

Preparation of blended PCL/PLGA materials. PCL (19561-500G, Mw 43,000–50,000; Polysciences) and PLGA (430471-5G, molar ratio of PLA to PGA 85:15, Mw 50,000–75,000; Sigma-Aldrich) were blended using a melting process.[26] Briefly, PCL and PLGA granules were melted and mixed in a glass container at 130°C for 10 min, where the mixing weight ratio was 1 to 1. The PCL/PLGA mixture was loaded into a 10-mL steel syringe installed in the dispensing head of the MHDS and maintained at 135°C for dispensing.

Preparation of collagen and gelatin solution encapsulating intact rhBMP-2. Clinically injectable 3% neutralized solution type atelocollagen (Koken) extracted from young calfskin was purchased. A 20% (w/v) gelatin solution was prepared by dissolving powdered gelatin (Yakuri Pure Chemicals) in deionized water. A 10 μg/mL aliquot rhBMP-2 solution was mixed with the collagen and gelatin solution for homogeneous distribution. All blending processes were conducted under aseptic condition. The relative volumes of aqueous rhBMP-2 solution and collagen or gelatin solution were adjusted to achieve the desired concentration. The rhBMP-2-loaded collagen and gelatin solutions were transferred into a sterilized 10-mL polypropylene (PP) syringe installed in another dispensing head of the four-head MHDS.

Three-dimensional printing-based scaffold fabrication using MHDS. Three-dimensional porous scaffolds were fabricated using two dispensing heads of the MHDS.[27] In the printing process, all labware including tweezers, slide glass, nozzle, and syringe was sterilized by UV exposure overnight prior to printing. Moreover, we did our best to keep the printing environment clean to retain the sterility. Therefore, during sterilization, the printed collagen and rhBMP-2 were not directly exposed to UV light, which might change the function of protein. We designed a hollow cylindrical scaffold for *in vitro* experiments. The outer and inner diameters of the scaffolds were fixed at 4 and 2 mm, respectively, while height of the scaffold was 3 mm. The internal empty space at the center of the scaffold was planned to be filled with the collagen or gelatin solution encapsulating intact rhBMP-2. The scaffold fabrication process for *in vitro* experiments consists of two sequential dispensing steps.[31] First, the blended PCL/PLGA fibers dispensed from the steel nozzle with a size of 250 μm were repeatedly deposited to construct the 3D porous scaffold where the fabrication temperature and pressure were 120°C and 650 kPa, respectively. Next, the end of the PP nozzle was placed at the center of the scaffold, and a collagen or gelatin solution with intact rhBMP-2 was sequentially dispensed into the hole. The temperature and pressure used for dispensing the collagen solution were 20°C and 30 kPa, respectively, whereas the temperature of the syringe was maintained at 37°C and the dispensing pressure was 60 kPa for dispensing the gelatin solution. The dispensed collagen solution was physically gelled at 37°C in the incubator for sustained delivery. In contrast, the dispensed gelatin solution quickly gelled at room temperature and was stored at 4°C without the cross-linking process to realize burst delivery. The scaffold whose shape was different from that of *in vitro* scaffold was separately fabricated by the same process introduced above for the *in vivo* experiments. The shape of the scaffold was specifically customized for the 20-mm segmental diaphyseal defect of a rabbit.

In vitro *release profile analysis of rhBMP-2*

PCL/PLGA scaffolds containing collagen or gelatin gel (loaded with intact rhBMP-2) were incubated in 10 mL phosphate-buffered saline (PBS) solution (pH 7.4) with 2.0 mM sodium azide and 0.01%(w/v) bovine serum albumin (BSA) at 37°C. Three different physical gelation times (0.5, 1, and 2 h) were used for collagen gel formation, whereas the gelatin gel was uncross-linked. Each scaffold was loaded with 15 ng of rhBMP-2. At predetermined points in time (day 1, 3, 5, 7, 14, 21, and 28), 1 mL of solution was harvested and stored at −20°C until quantification. The solution was replaced with a similar volume of fresh buffer. Sterile conditions were applied to prevent any contamination of the samples. The release amount of the total rhBMP-2 was determined by an enzyme-linked immunosorbent assay (ELISA) development kit specific for rhBMP-2 (Peprotech) according to the manufacturer's protocol. A calibration curve was obtained using standard preparations of rhBMP-2 of known concentration. Each sample was assayed in triplicate ($n=3$) and means ± standard deviation (SD) values were reported.

In vitro *cellular activity test*

Cell isolation. hTMSCs were isolated as described previously.[28–30] The isolation procedures were approved by the Institutional Review Board of Seoul St. Mary's Hospital, the Catholic University of Korea (KC08TISS0341). Briefly, inferior turbinate tissues were obtained from a patient who underwent partial turbinectomy with an informed consent before surgery. The inferior turbinate tissue obtained after surgery was washed five times with saline solution containing gentamicin (Kukje Pharmaceutical Industries). The inferior turbinate tissue was washed at room temperature thrice with antibiotic-antimycotic solution (Gibco) and twice with PBS, and then cut into 1 mm^3 pieces. The pieces were placed into a culture dish, and the dish was covered with a sterilized glass cover slide. Dulbecco's modified Eagle's medium (Gibco) containing 10% fetal bovine serum was added, and the tissues were incubated at 37°C in a 5% CO_2 atmosphere. After 3 weeks of culture, the glass cover slide was removed, and tissues floating in the culture medium were removed by washing. The hTMSCs that had attached to the bottom of the culture dish were detached using 3 mL of 0.25% trypsin in 1 mM EDTA. The hTMSCs were cultured to the third passage for use in experiments.

Cell seeding and culture. The isolated hTMSCs were seeded onto the PCL/PLGA/collagen/rhBMP-2 (rhBMP-2 concentrations of 0, 0.5, 1.5, 4.5, 5.0, and 7.5 μg/mL) and PCL/PLGA/gelatin/rhBMP-2 (rhBMP-2 concentrations of 0, 5.0 μg/mL) by pipetting 10 μL of a cell suspension containing 1×10^5 cells.[30] Before seeding the cells, the sterilized scaffolds were prewetted in culture medium for 3 h. Osteogenic medium containing 50 μM l-ascorbic acid-2-phosphate (Sigma Aldrich), 10 mM β-glycerophosphate (Sigma Aldrich), and 100 nM dexamethasone (Sigma Aldrich) in complete alpha minimum essential medium was used to induce the osteogenic differentiation of the hTMSCs, and the culture medium was changed every 2 days.

RNA extraction and real-time PCR of hTMSCs on the rhBMP-2-loaded scaffolds. Total RNA was extracted from the hTMSCs and seeded onto the 3D printing-based scaffold having various rhBMP-2 doses (in triplicate), using TRIzol reagent (Invitrogen) and was reverse-transcribed with SuperScript II Reverse Transcriptase (Invitrogen) at day 14 after treatment with osteoblast differentiation medium. The expression of osteoblast marker genes such as *alkaline phosphatase (ALP)* and *osteocalcin (OC)* was analyzed using real-time quantitative reverse transcription–polymerase chain reaction (RT-PCR). The amplification primers were designed for human *ALP* (5′ primer, ATG TCA TCA TGT TCC TGG GAG AT; 3′ primer, TGG AGC TGA CCC TTG AGG); human *OC* (5′ primer, AAC CCA CGA ATG CAC TAT CCA; 3′ primer, CGG ACA TAC CGA GGG ACA TG); and human GAPDH (5′ primer, CCA GGT GGT CTC CTC TGA CTT C; 3′ primer, GTG GTC GTT GAG GGC AAT G). Real-time PCR analysis using SYBR Green was conducted with a Light Cycler 2.0 (Roche).

In vivo *new bone formation in a rabbit radius defect*

Experimental animals. Thirty healthy male New Zealand white rabbits, 12 weeks of age and weighing 3.3–3.5 kg were used. They were purchased from Samtaco Bio Korea experimental animal breeding center. All rabbits were kept in private cages in an air-conditioned environment (room temperature 20°C ± 2°C, humidity 40–60%) and illuminated between 08:00 and 20:00 (150–300 Lux) in the laboratory animal research center of Chungbuk National University (CBNU). All rabbits were fed with a commercial pellet diet (Sam Yang Feed Co.) during the entire study period. The thirty rabbits were randomly divided into three groups, with ten animals in each group. The three experimental groups were PCL/PLGA scaffolds (group 1), PCL/PLGA/gelatin/rhBMP-2 scaffolds (group 2), and PCL/PLGA/collagen/rhBMP-2 scaffolds (group 3). Five out of the 10 animals were sacrificed at week 4, and another 5 animals at week 8.

Surgical procedure. Prior to surgery, the rabbits were fasted for 12 h to prevent any possible adverse effects associated with anesthesia. The rabbits were premedicated by the subcutaneous injection of 0.05 mg/kg of atropine sulfate (Atropine Sulfate; Huons), 10 mg/kg of enrofloxacin, and an intramuscular injection of 3 mg/kg of ketoprofen (UniketoPro INJ; UNIBIOTech). Anesthesia was performed with 5 mg/kg of xylazine hydrochloride (Rompun®; Bayer Korea) and 35 mg/kg of ketamine HCl (Ketar®; Yu-han Yanghang Co. Ltd.) by intramuscular injection.

The surgical area was shaved and disinfected with 70% ethanol and povidone-iodine solution. Under sterile conditions, a longitudinal incision was made along the radius. The radius was exposed by dissecting the muscles. A segmental defect of 20 mm was created in the middle of the radius using an oscillating saw. The 20-mm-long scaffolds were placed on the radius defect without an outer fixture. The incision was then closed. Postoperatively, 5 mg/kg of enrofloxacine (Baytril®; Bayer Korea) and 2.2 mg/kg of carprofen (Rimadyl®; Pfizer Animal Health) was administered orally twice daily for 7 days. Fifteen animals were sacrificed at week 4, and the other 15 at week 8.

Analysis of *in vivo* bone formation. The degree of bone formation was investigated by microcomputed tomography

(μCT, Skyscan 1173; Skyscan) and histological analyses with hematoxylin–eosin (H&E) and Masson's trichrome (MT) staining. The new bone volume (NBV) and bone mineral density (BMD) of the samples were analyzed using the μCT Analyzer (ver. 1.4; Skyscan).

Immunofluorescence staining for confirmation of inflammatory response. To detect macrophage in the site of scaffold transplanted, we performed immunofluorescence staining for F4/80 using paraffin sections. Paraffin sections were deparaffinized and fixed with 10% formalin for 1 h. After blocking with 1% (w/v) BSA for 1 h, tissue slides were incubated overnight with fluorescently conjugated F4/80 antibody (1:200, #53-4801; eBioscience). After washing thrice with PBS buffer, stained slides were mounted with mounting medium with DAPI (#E19-18; GBI-Golden Bridge International) and observed under a confocal microscope (LX71; Olympus).

Scanning electron microscope

The morphology of the 3D printing-based scaffolds was observed using a scanning electron microscope (SEM, JSM-5300; JEOL) at 10 kV. The scaffolds were freeze-dried and coated with gold using a sputter coater for 15 s.[32]

Statistical analysis

All data were expressed as mean ± SD. Tukey's *post hoc* test of one-way analysis was performed using MINITAB ver. 14.2 software. Values of $p < 0.05$ were considered to be statistically significant.[33]

Results and Discussion

Scaffold fabrication for in vitro *and* in vivo *experiments*

The 3D printing-based scaffolds releasing intact rhBMP-2 were successfully fabricated using the MHDS equipped with four dispensing heads having individual temperature and pneumatic pressure controllers (Fig. 1). It was previously demonstrated that the MHDS is an effective 3D printing system for dispensing various biomaterials including synthetic polymers and natural hydrogel into a 3D scaffold for tissue engineering.[30] In this study, a cylindrical hollow 3D scaffold with 4 mm of outer diameter, and 2 mm of inner diameter was intentionally designed for *in vitro* experiments (Fig. 2A). The line width and pore size of the PCL/PLGA hollow cylindrical 3D scaffold were 150 and 250 μm, respectively (Fig. 2A). After completing the fabrication of the PCL/PLGA scaffold, the internal empty space of the scaffold was filled with collagen or gelatin solution containing rhBMP-2 using another dispensing head of the MHDS with a single injection (Fig. 2B). After calculating the volume of the internal space with computer aided design (CAD) modeling, it was found that ~10 μL of collagen or gelatin solution could be consistently injected into the internal space using the MHDS. It was observed that the collagen was placed in the internal space with no excess (Fig. 2C).

In addition, 3D scaffolds resembling the 20-mm-long rabbit diaphyseal defects were fabricated using the MHDS for *in vivo* experiments. The 3D CAD modeling of a rabbit radius and ulna was prepared before fabrication (Fig. 2D). Then, the CAD model was converted into a G-code using software developed in house.[10] The 3D scaffolds for the *in vivo* experiments were also designed for the hollow cylindrical PCL/PLGA scaffolds where the gel with rhBMP-2 was dispensed into the internal space (Fig. 2D). The scaffold fabrication process specified for the *in vivo* experiment was described in Figure 2E–G. The PCL/PLGA fibers were deposited with a layer-by-layer process to form a 3D scaffold until the internal space of the scaffold was not entirely closed in the vertical direction of the working substrate (Fig. 2E). The unclosed internal space was filled with the gel using another dispensing head of the MHDS (Fig. 2F). After that, the rest of the PCL/PLGA part was completely fabricated (Fig. 2G). Porous PCL/PLGA scaffolds for *in vivo* experiments were successfully fabricated (Fig. 2H). The internal space at the center of the scaffold (Fig. 2H) and PCL/PLGA/collagen scaffolds with internal spaces filled with collagen gel were observed using SEM (Fig. 2I). The volume of the dispensed gel for the *in vivo* experiments was fixed at 50 μL. There was no excess of gel over the holes (Fig. 2I). The consistency of the dispensing volume of the gel with rhBMP-2 could be very important for bone tissue engineering. It is well known that the total dose of rhBMP-2 sensitively affects the osteogenesis.[33] Therefore, the precise control of the rhBMP-2 dose should be guaranteed. Otherwise, osteogenesis behavior could be unpredictable. In that sense, the scaffolds fabricated by the MHDS enabling consistent dispensing of biomaterials could be advantageous for obtaining reliable information on rhBMP-2 in bone regeneration.

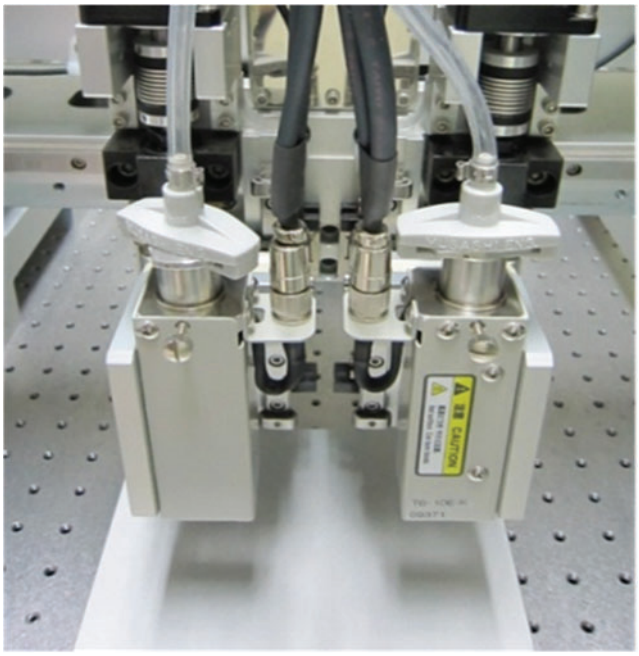

FIG. 1. Images of multi-head deposition system (MHDS). Color images available online at www.liebertpub.com/tea

In vitro *release profile of rhBMP-2 from PCL/PLGA/collagen and PCL/PLGA/gelatin scaffolds*

The *in vitro* release profile of encapsulated rhBMP-2 from PCL/PLGA/collagen and PCL/PLGA/gelatin scaffolds was investigated. The PCL/PLGA scaffold filled with collagen

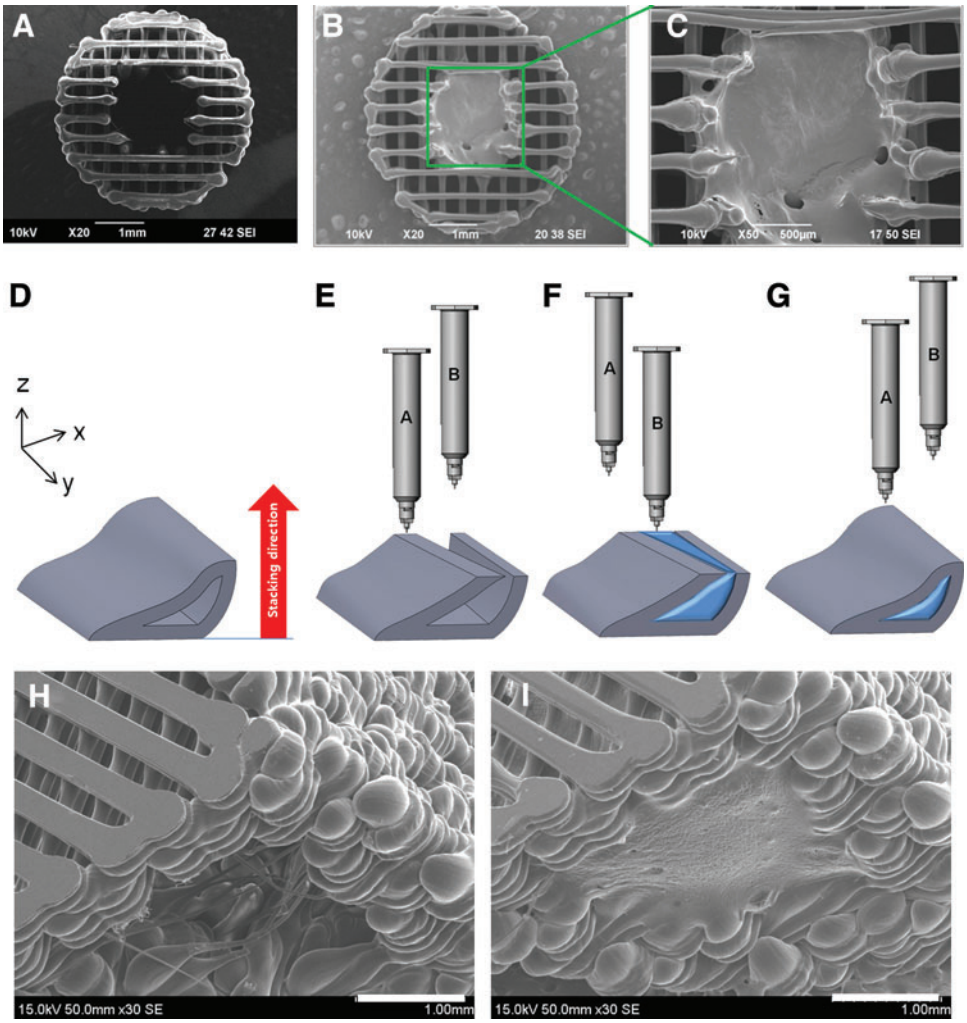

FIG. 2. Fabricated scaffold for *in vitro* experiments: **(A)** No gel polycaprolactone (PCL)/poly(lactic-co-glycolic acid) (PLGA) scaffold, **(B)** PCL/PLGA/collagen hybrid scaffold, **(C)** atelocollagen gel inside the PCL/PLGA scaffolds (magnified image). Fabrication process of three-dimensional (3D) PCL/PLGA/hydrogel using the MHDS: **(D)** computer aided design modeling for the radius of a rabbit segmental defect, **(E)** first step in building the porous PCL/PLGA framework, **(F)** dispensing of hydrogel solution encapsulating growth factors into open spaces of a PCL/PLGA framework. **(G)** Fabrication of incomplete parts of PCL/PLGA framework. Fabricated scaffold for *in vivo* experiments and isometric scanning electron microscope views of **(H)** the PCL/PLGA and **(I)** PCL/PLGA/collagen. Color images available online at www.liebertpub.com/tea

gel showed an initial burst release of rhBMP-2 during the first 24 h (~20%), possibly due to nonencapsulated rhBMP-2 on the surface of the gel (Fig. 3).

After the initial burst release, the release showed controlled delivery over time for all the three types of the collagen gel-based scaffolds. The collagen gels cross-linked for 0.5 h at 37°C showed a faster release rate compared with the gels cross-linked for 1 and 2 h. The burst release of the rhBMP-2 at 37°C from the uncross-linked gelatin gel was evident. The release profile showed that ~88% of the loaded rhBMP-2 was released within 24 h from the PCL/PLGA/gelatin scaffolds. The remaining rhBMP-2 was released subsequently and almost the entire quantity of rhBMP-2 was released within a week from the gelatin gels. The possible mechanisms hindering the release of proteins from the collagen structures might be due to reduced degradability, and electrostatic interactions between entrapped proteins and cross-linked collagen meshwork.[35] The desired dosage for inducing bone formation can be greatly reduced when rhBMP-2 is combined with an appropriate delivery system that retains rhBMP-2 at the grafted site sufficient for inducing bone formation.[36,37] The release kinetics of the rhBMP-2 from the delivery system (hydrogel matrix) and the retention of its biological activity are critical factors for successful and efficent *in vivo* bone formation.[38] Overall, rhBMPs are components of the biologically inspired strategies aiming to promote and facilitate the bone healing process in critical-sized bone defects.

Effect of rhBMP-2 dose and release rate on in vitro *osteogenic differentiation*

Effective rhBMP-2 dose for *in vitro* osteogenic differentiation of hTMSCs. Effects of rhBMP-2 released from the PCL/PLGA/collagen and PCL/PLGA/gelatin scaffolds on the osteogenic differentiation of hTMSCs were investigated by measuring the gene expression levels of *ALP* and *OC* from the cells. The *ALP* and *OC* expression levels of the hTMSCs seeded on the 3D scaffolds were detected by RT-PCR at day 14 after seeding. To determine an effective dose of rhBMP-2 loaded on the PCL/PLGA/collagen scaffold, four different scaffolds with different rhBMP-2 concentrations of 0, 1.5, 4.5, and 7.5 μg/mL were prepared. As seen in Figure 4A, relative gene expression levels of *ALP* from the hTMSCs on the scaffolds with rhBMP-2 concentrations of 0, 1.5, 4.5, and 7.5 μg/mL were 1 ± 0.02, 2.45 ± 0.29, 2.60 ± 0.57, and 3.13 ± 0.43, respectively. The *ALP* expression levels in the scaffolds having 1.5, 4.5, and 7.5 μg/mL of rhBMP-2 were significantly higher than those in the scaffolds without rhBMP-2. However, there was no significant

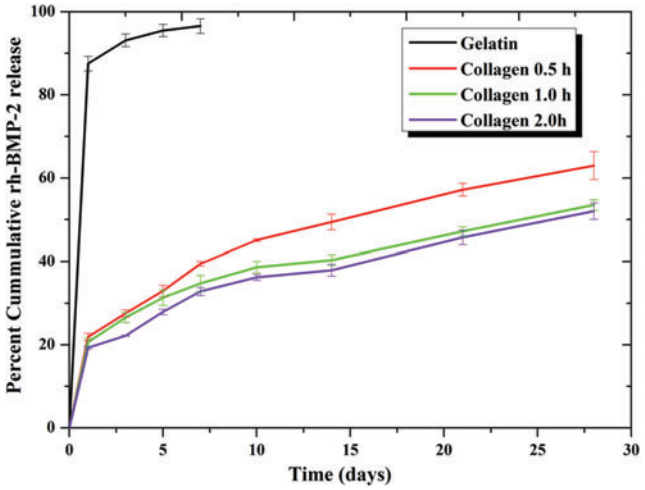

FIG. 3. *In vitro* recombinant human bone morphogenetic protein-2 (rhBMP-2) release profile from the 3D printing-based PCL/PLGA/hydrogel scaffolds. Approximately 88% of rhBMP-2 loaded on the PCL/PLGA/gelatin scaffolds was initially release within 24 h. In contrast, the controlled release of rhBMP-2 up to 28 days was measured from the PCL/PLGA/collagen scaffolds. The procedure was performed in triplicate. Color images available online at www.liebertpub.com/tea

difference in *ALP* expression levels between scaffolds with 1.5, 4.5, and 7.5 μg/mL of rhBMP-2. Meanwhile, the *OC* gene expression levels from the hTMSCs on the scaffolds with rhBMP-2 concentrations of 0, 1.5, 4.5, and 7.5 μg/mL were 1 ± 0.23, 7.47 ± 2.14, 12.60 ± 1.40, and 14.47 ± 0.81, respectively. The *OC* expression levels of the hTMSCs on the scaffolds with rhBMP-2 were also significantly higher than those of the hTMSCs on the scaffolds without the rhBMP-2 (Fig. 4B).

In contrast to the result of *ALP*, the *OC* expression levels of the hTMSC on scaffolds with 4.5, and 7.5 μg/mL of rhBMP-2 were significantly higher than those of the hTMSCs on the scaffolds with 1.5 μg/mL (Fig. 4B). However, the effect of 4.5 and 7.5 μg/mL of rhBMP-2 on *OC* expression of hTMSCs was not significantly different from each other (Fig. 4B). This indicates that an rhBMP-2 dose higher than 4.5 μg/mL could actively promote the induction of osteogenic differentiation of hTMSCs *in vitro*. However, it was reported that an rhBMP-2 dose exceeding an optimal dose did not ensure a greater degree of osteogenic differentiation of MSCs *in vitro*.[39] Therefore, it is recommended that the dose of rhBMP-2 be minimized as far as possible due to its high cost and possible adverse effects of rhBMP-2, if the threshold dose can be determined.[40] Hence, 5.0 μg/mL of rhBMP-2, which is one of the commonly used doses in rhBMP-2 study, was determined to be an effective dose for promoting the osteogenic differentiation of hTMSCs in 3D printing-based scaffolds.

Effect of the rhBMP-2 release rate on *in vitro* osteogenic differentiation of hTMSCs. To show the effect of the release rate of rhBMP-2 on osteogenic differentiation of hTMSCs, collagen and gelatin solutions were used for sustained and burst rhBMP-2 delivery systems, repectively. The 5.0 μg/mL of rhBMP-2 was encapsulated in both collagen and gelatin solutions. *ALP* and *OC* expression levels of hTMSCs seeded on the PCL/PLGA/collagen and PCL/PLGA/gelatin scaffolds with and without rhBMP-2 were measured by RT-PCR at day 14 after the initial seeding. In *ALP* and *OC* gene expression levels, there were no significant differences between PCL/PLGA/gelatin scaffolds with and without rhBMP-2 (Fig. 4C, D). This means that the burst release of rhBMP-2 did not affect the induction of the osteogenic differentiation of hTMSCs. On the other hand, a sustained release of rhBMP-2 with a concentration of 5.0 μg/mL

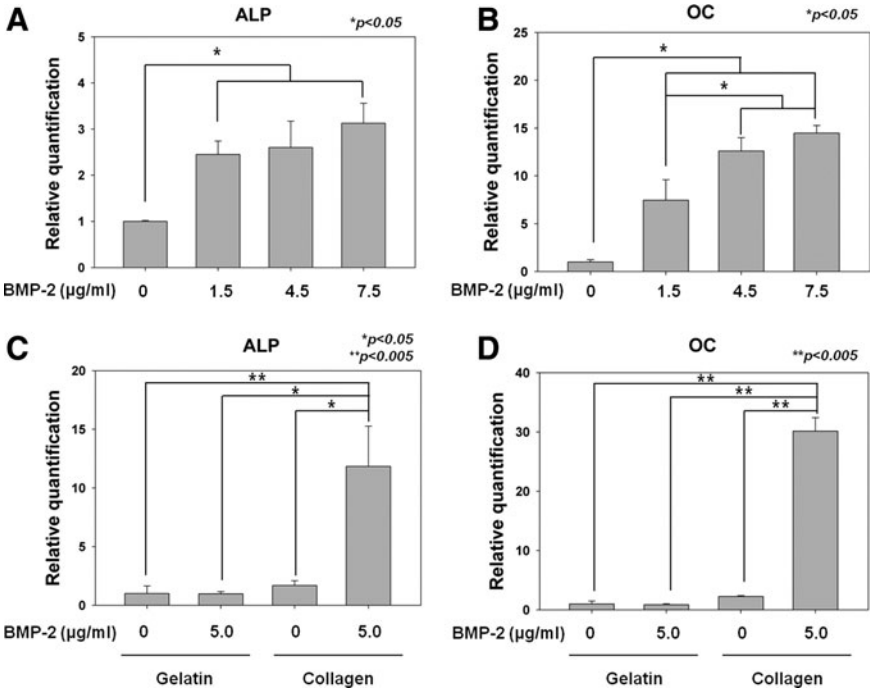

FIG. 4. Normalized gene expression levels of *alkaline phosphatase (ALP)* and *osteocalcin (OC)* from the human nasal inferior turbinate-derived mesenchymal stromal cells seeded on the PCL/PLGA/collagen/rhBMP-2 and PCL/PLGA/gelatin/rhBMP-2 for investigation of the optimal dose **(A, B)** and release rate **(C, D)** at day 14 after seeding $*p < 0.05$, $**p < 0.005$.

from the PCL/PLGA/collagen scaffold showed 7 and 13 times higher *ALP* and *OC* expression levels, respectively, compared with the PCL/PLGA/collagen scaffold without the rhBMP-2 (Fig. 4C, D). It was confirmed that the bioactivity of rhBMP-2 from the 3D printing-based scaffolds was intact. The fabrication process did not cause denaturation of the loaded proteins. In addition, the *ALP* and *OC* expression levels of the sustained releasing system were 12 and 35 times higher, respectively, than those of the burst releasing system at an equivalent concentration (Fig. 4C, D). These results could be interpreted as follows: RhBMP-2 is known to promote the osteogenic differentiation of MSCs at an early stage, and to upregulate the calcification of bone defects.[41] However, ~90% of rhBMP-2 was initially released within 24 h from the PCL/PLGA/gelatin scaffolds. Moreover, the osteogenic media for culturing the hTMSCs were changed every 2 days. Therefore, most of the burst released rhBMP-2 from the gelatin gel could have been washed away by the medium change at day 2. The osteogenic induction effect might have thereby been diminished.

In vivo *new bone formation results according to the different release rates of rhBMP-2 from 3D printing-based scaffolds*

A segmental defect of 20 mm was created in the middle of the radius using an oscillating saw under copious irrigation with saline solution (Fig. 5A). The 20-mm size of the segmental diaphyseal defect could have been a more challenging critical defect size for a rabbit compared with the sizes used in other studies.

The sterilized scaffolds of groups 1, 2, and 3 were placed into the defect. A negative control group (defect only), which has been widely reported on, was intentionally excluded to reduce the number of experimental animals. The 20-mm scaffolds were very well matched with the size of the defects (Fig. 5B). The implanted scaffolds and native bone were tightly connected to each other with no gap. The tightness of the contact between the scaffold and native bone can significantly affect the bone formation. It is reported that 3D scaffolds play an important role as matrices for attachment and proliferation of anchorage-dependent osteoblasts, which tend to grow over the scaffolds.[42] Therefore, new bone formation can occur outward from the native bone when the scaffolds meet the native bone with no gap. In this respect, the 3D printing technology enabling the fabrication of a customized 3D scaffold with complex geometry is superior to other traditional methods for manufacturing 3D scaffolds. In addition, no remaining bone debris was observed in radiographs taken immediately after implantation at the defect site (Fig. 5C). Any remaining bone debris produced by surgery can facilitate new bone formation itself, which can produce misleading experimental results.[43] The μCT analysis was carried out to evaluate the bone formation at both weeks 4 and 8 after surgery (Supplementary Videos S1–S6; Supplementary Data are available online at www.liebertpub.com/tea).

Little bone formation was observed in group 1 or 2 at week 4 (Fig. 6A, B). Interestingly, despite substantial use of rhBMP-2 (5 μg/mL), the defect site of group 2 remained almost empty at week 4 (Fig. 6B). In comparison, new bone formation, which was thought to have been generated from the native radius parts, was obviously observed in group 3 at week 4 (Fig. 6C). At week 8 after surgery, newly regenerated bone was detected at the defect site in group 1 (Fig. 6D). Notably, new bone was observed at the interface between the radius and ulna in group 1. New bone formation tends to progress from native bone tissues surrounding the defect.[44] The progress in bone healing observed in group 2 at week 8 was remarkable compared to that of week 4

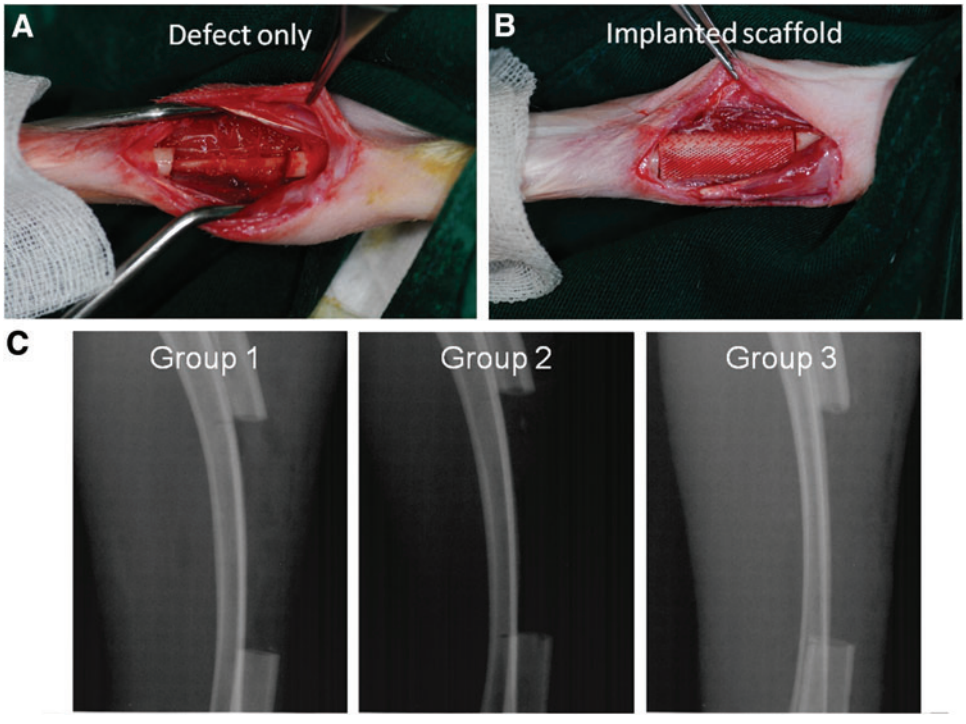

FIG. 5. **(A)** *In vivo* rabbit radius segmental defect, and **(B)** implanted scaffold at the 20-mm defect site. **(C)** Two-dimensional X-ray images taken immediately after implantation at the defect site. It was confirmed that no remaining bone debris was observed at the defect site. Color images available online at www.liebertpub.com/tea

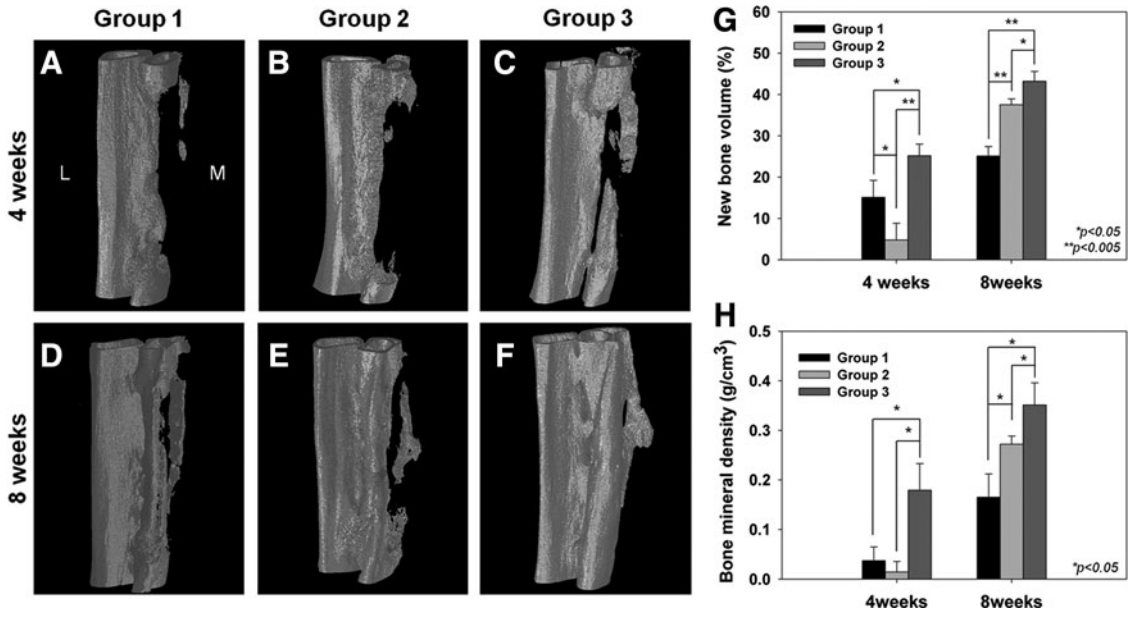

FIG. 6. Microcomputed tomography images were taken at weeks 4 **(A–C)** and 8 **(D–F)** after surgery. **(A, D)** group 1, **(B, E)** group 2, **(C, F)** group 3. Quantitative analyses including new bone volume **(G)** and bone mineral density (BMD) **(H)** for the *in vivo* experiments were performed (repeated five times). In Figure 8A, L and M indicate lateral and medial, respectively.

(Fig. 6E). The 20-mm defect site was partially regenerated by newly formed tissue that appeared to be ''bone,'' and the new bone was fused with the native bone parts such as the ulna and remaining radius (Fig. 6E). However, it seems that the posterior area of the radius still needed to be regenerated more extensively (Fig. 6E). Group 3 demonstrated outstanding new bone formation at week 8. Both ends of the native radius bone had been completely bridged by newly regenerated bone, and the new bone exhibited complete bony fusion with the native bone (Fig. 6F). The quantitative analyses of the NBV and BMD were performed using software with the μCT, in which NBV indicates a ratio of the NBV to the defect volume. The NBV and BMD values are presented in Figure 6G and H, respectively. The NBV values in groups 1, 2, and 3 at 4 weeks after surgery were 15.11 ± 4.08, 4.77 ± 4.06, and $25.17\% \pm 2.83\%$, respectively (Fig. 6G). The NBV of group 3 was significantly higher than that of group 1 ($p < 0.05$) and group 2 ($p < 0.005$). It is to be noted that the NBV of group 2 was significantly lower than that of group 1, which did not even use the rhBMP-2. It may have been that the burst release of rhBMP-2 exhibited an adverse effect on new bone formation until week 4 after surgery. In contrast, group 3 with the sustained release of rhBMP-2 showed 1.67 and 5.28 times higher NBV values than group 1 and group 2. In addition to NBV, the BMD values indicating the degree of calcification were evaluated. The BMD values of groups 1, 2, and 3 at week 4 after surgery were 0.037 ± 0.028, 0.014 ± 0.021, and $0.179 \pm 0.054\,g/cm^3$, respectively (Fig. 6H). The BMD of group 3 was significantly higher than that of groups 1 and 2 ($p < 0.05$). There was no significant difference between group 1 and 2. The higher BMD values of group 3 might be ascribed to the sustained release of rhBMP-2 promoting the osteogenic differentiation process including the calcification of MSCs.

At week 8 after surgery, the NBV value of group 3 ($43.17\% \pm 2.43\%$) was significantly higher than that of group 1 ($25.13\% \pm 2.26\%$, $p < 0.005$) and group 2 ($37.53\% \pm 1.40\%$, $p < 0.05$) (Fig. 6G). In particular, the NBV value of group 2 showed a rapid and substantial increase (7.87-fold) at week 8 compared with that of week 4. The NBV of group 2 was significantly higher (1.5-fold) than that of group 1 at week 8 ($p < 0.005$). In addition, the BMD values at week 8 after surgery showed a similar tendency with the NBV. The BMD values of groups 1, 2, and 3 were 0.165 ± 0.047, 0.272 ± 0.017, and $0.351 \pm 0.044\,g/cm^3$, respectively (Fig. 6H). There was a significant difference between each of the groups ($p < 0.05$). Moreover, both the NBV and BMD values of group 3 at week 4 were comparable to those of group 1 at week 8. From these results, it can be concluded (stated) that the sustained release of rhBMP-2 as in group 3 accelerates bone formation, resulting in a far reduced healing period.

Meanwhile, the bone formation of groups 1, 2, and 3 was also analyzed by histological analyses with H&E and MT stainings (Fig. 7). A cross section of the implanted scaffold and ulna was stained and observed. In both H&E and MT stainings, there was no noticeable new bone formation inside the scaffolds of groups 1 and 2 at week 4 (Fig. 7A, B, D, E). Instead, little new bone formation was observed in the space between the scaffold and ulna. In particular, a mass of soft tissue was observed in the vicinity of the scaffolds in group 2 at week 4 (Fig. 7B, E). On the other hand, active new bone formation was markedly observed even inside of the scaffold and around it in group 3 (Fig. 7C, F). At week 8 after surgery, calcified and matured new bone that infiltrated into the scaffolds was observed in all of the groups (Fig. 7G–L). In group 1, a substantial amount of new bone was observed in the interface between the ulna and radius (Fig. 7G, J). Further, an ingrowth of new bone inside the scaffold

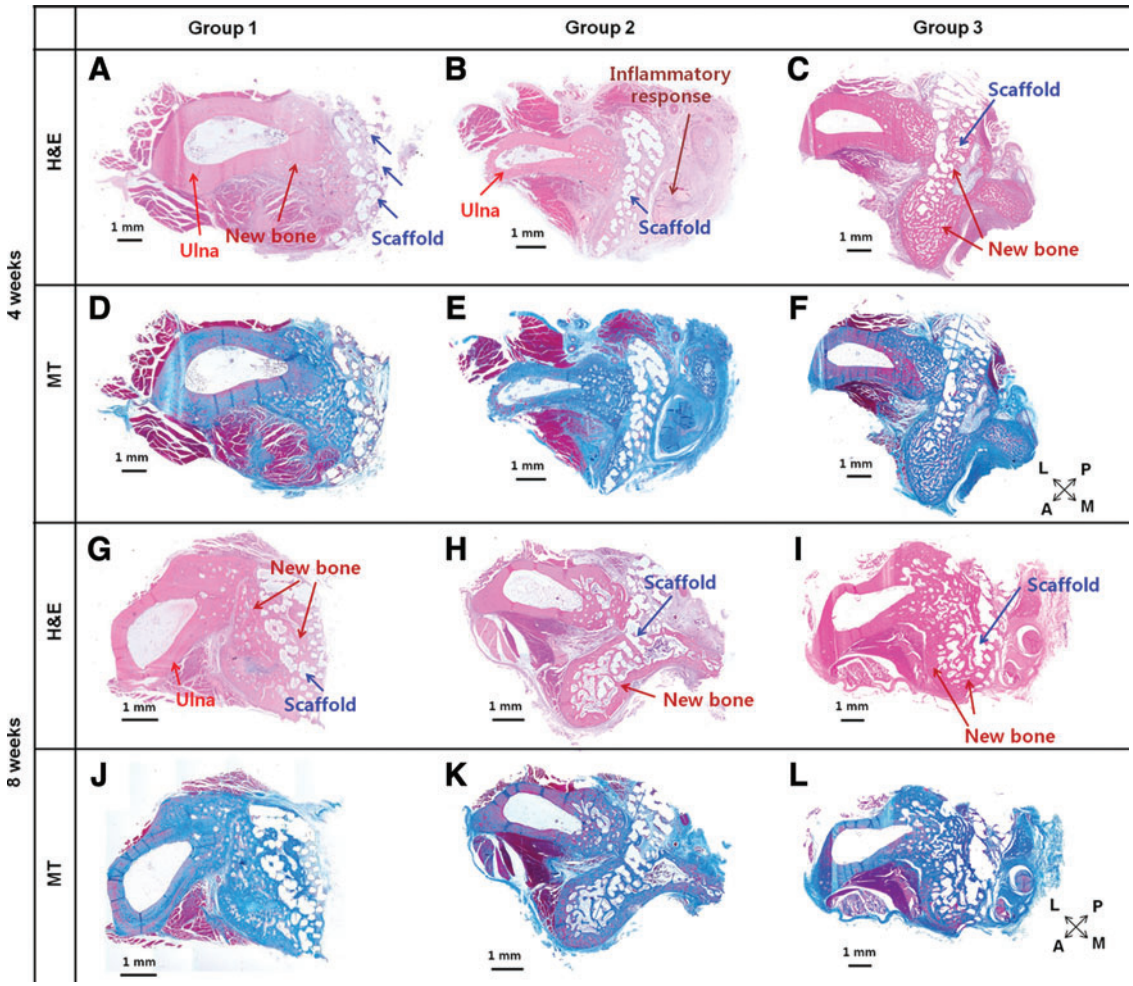

FIG. 7. Histological analyses of regenerated bones at week 4 with hematoxylin–eosin (H&E) staining **(A–C)** and Masson's trichrome (MT) **(D–F)** of groups 1 **(A, D)**, 2 **(B, E)**, and 3 **(C, F)** from the radius segmental defects in rabbits. In particular, massive soft tissue where a large number of neutrophils were densely recruited was observed in the vicinity of group 2. Histological analyses of regenerated bones at week 8 with H&E staining **(G–I)** and MT **(J–L)** of groups 1 **(G, J)**, 2 **(H, K)**, and 3 **(I, L)** from the radius segmental defects in rabbits. Matured and calcified bone regeneration was observed in all of the groups. However, the degree of bone formation was the best in group 3. In the lower-right corner, L, M, P, and A indicate lateral, medial, posterior, and anterior, respectively. Color images available online at www.liebertpub.com/tea

was also observed. The active ingrowth of bone inside the scaffold can be attributed to the fully interconnected pores, which is an intrinsic characteristic of the 3D printing-based scaffold.[45] However, the ingrowth of new bone that might have started from the ulna did not reach the periphery of the radius (far away from the ulna), which was consistent with the Figure 6D (Fig. 7G, J). Group 2 exhibited corticalized bone formation along the border of the scaffold at week 8 in both H&E and MT stainings (Fig. 7H, K). As mentioned in Figure 6E, newly regenerated tissue on the posterior side of the radius was premature (Fig. 7H, K). On the other hand, considerably mature bone formation could be clearly observed throughout the scaffolds in group 3 (Fig. 7I, L). Overall, the sustained release of rhBMP-2 of 5 μg/mL from the 3D printing-based scaffolds remarkably promoted and accelerated new bone formation without adverse effects until week 8 after surgery. The 3D printing-based PCL/PLGA scaffold (group 1) itself also showed the promising possibility for regenerating new bone tissue. However, it seems that a healing period of 8 weeks was insufficient to heal the 20-mm radius defect using the scaffolds of group 1. Interestingly, the NBV of group 2 (5 μg/mL with burst release) was significantly lower than that of group 1 (no rhBMP-2) and group 3 (5 μg/mL with burst release) at week 4, whereas the NBV and BMD values of group 2 were higher than those of group 1 at week 8. The degree of new bone formation may have rapidly increased from week 4 to 8. The curiosity of this phenomenon was solved by the histological and immunohistochemical analyses in Figures 8 and 9. Massive soft tissue was specifically observed in the vicinity of the scaffolds in group 2 (Fig. 8A).

It was noted that a large number of macrophages were recruited into the soft tissue, indicating severe inflammation (Fig. 8B, C). In addition, the presence of macrophages in the soft tissue around the scaffold was also confirmed by the immunohistochemical staining analysis, in which F4/80 molecules were stained by green fluorescence. The F4/80 molecule is known to be expressed by a variety of

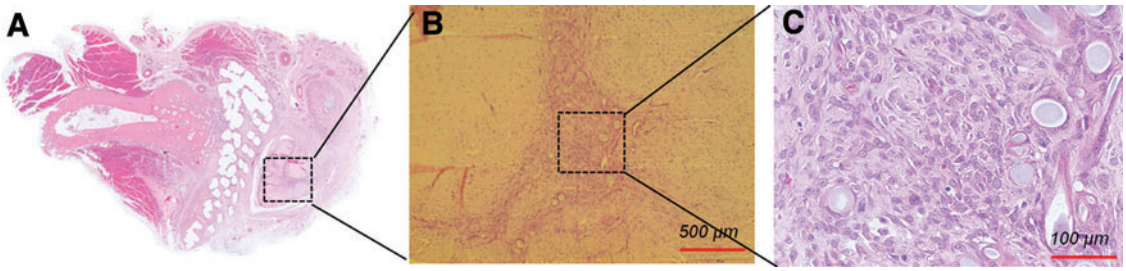

FIG. 8. H&E staining result of group 2 at week 4 **(A)**. Magnified views **(B, C)** of massive soft tissue found in the vicinity of the scaffolds in group 2 at week 4. The recruited cells were identified as typical macrophages indicating a typical inflammatory response. Color images available online at www.liebertpub.com/tea

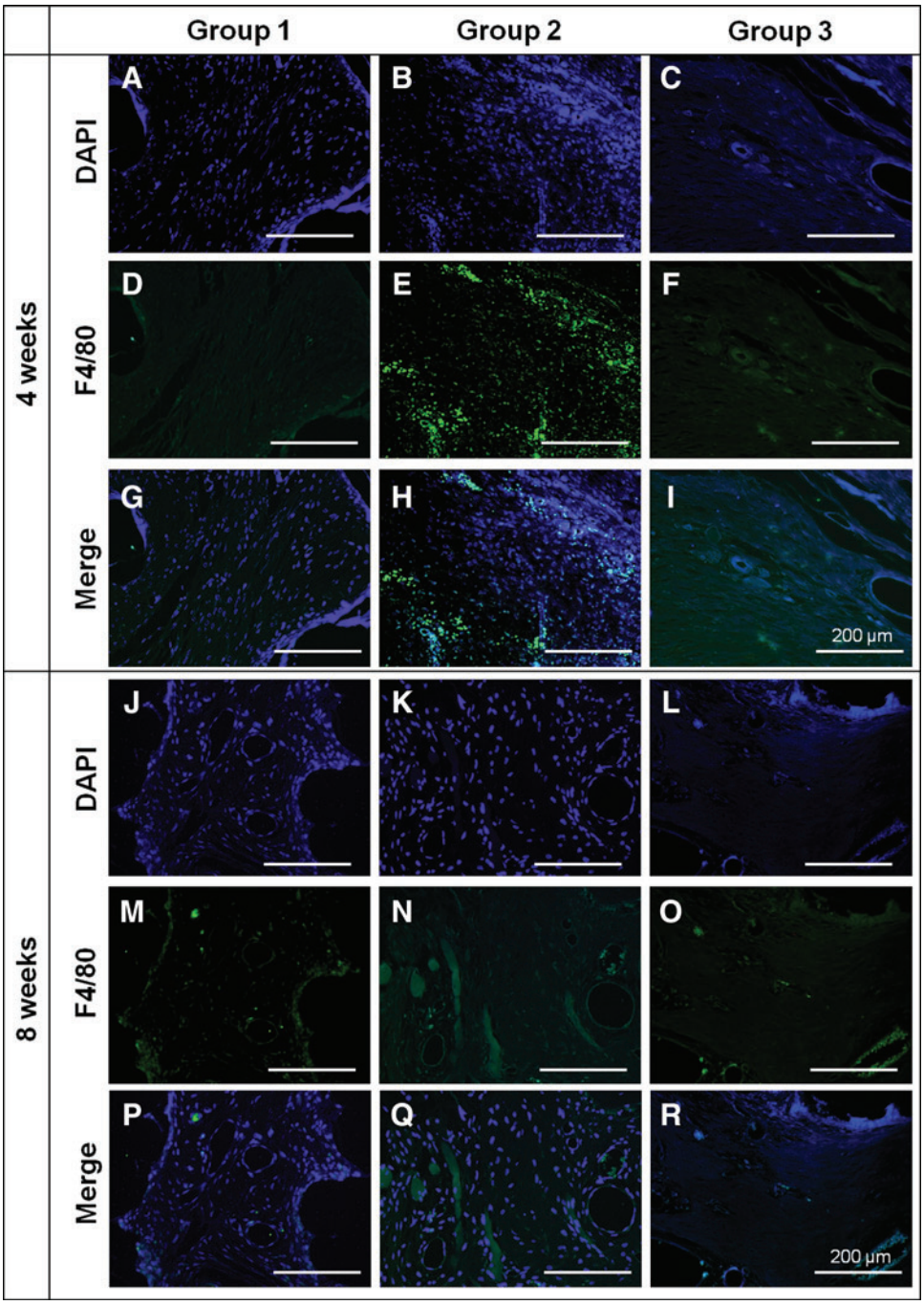

FIG. 9. Immunohistochemical staining results of soft tissue in the vicinity of the scaffolds. DAPI **(A–C,** and **J–L)** and F4/80 **(D–F,** and **M–O)** staining exhibit blue and green fluorescence, respectively. Merged images **(G–I,** and **P–R)** were also shown. Large number of cells were particularly detected in group 2 **(B)** compared to group 1 **(A)** and 3 **(C)** at week 4. Moreover, highly expressed green fluorescence was clearly observed at the same site where the large number of cells were detected in group 2 **(E)** at week 4, while that was not observed in group 1 **(D)** and 3 **(F)**. On the other hand, there was no significant F4/80 expression in any of the groups at week 8 **(M–O)**. Color images available online at www.liebertpub.com/tea

macrophages.[46] As shown in Figure 9, a large number of cells identified by DAPI staining were particularly observed in group 2 (Fig. 9B) at week 4, whereas few cells were detected in groups 1 (Fig. 9A) and 3 (Fig. 9C).

Moreover, F4/80 (stained by green fluorescence) was highly expressed at the same site where the large number of cells were observed (Fig. 9E) in group 2 at week 4. Thus, it is obvious that the recruited cells in the soft tissue were macrophages as we supposed. Interestingly, F4/80 expression was not detected in group 2 at week 8 (Fig. 9N). On the other hand, no significant expression of F4/80 was observed in group 1 (Fig. 9D, M) or in group 3 (Fig. 9F, O) at either week 4 or 8. Hence, the poor bone regeneration of group 2 at week 4 could be ascribed to the severe inflammatory response provoked by the burst release of rhBMP-2. It has been reported that rhBMP-2 can induce an exaggerated inflammatory reaction resulting in massive edema and subsequent axillary vein compression at an early stage.[47] Moreover, the severe inflammatory response is known to inhibit bone regeneration.[48] Therefore, it could be concluded that the burst release of 5 μg/mL rhBMP-2 can hinder new bone formation at an early stage by provoking an inflammatory response. Additionally, it was reported that the inflammatory response provoked by a treatment of rhBMP-2 had completely resolved within a few weeks after the treatment.[47] That is, the inflammatory response provoked at the early stage had been naturally alleviated after 4 weeks. At the same time, it has been reported that a modulation of the pro-inflammatory cytokines expressed by inflammatory cells has a capacity to stimulate osteogenesis.[48,49] Indeed, in the case of group 2, the bone formation was surprisingly increased at week 8, although it was the poorest at week 4. It is believed that the alleviated inflammatory response after week 4 may have played an important role in the rapid bone regeneration at week 8 in group 2. Therefore, it is concluded that the burst release of rhBMP-2 can provoke an inflammatory response that could hinder new bone formation at an early stage, but bone regeneration could be strongly stimulated as the inflammatory response is gradually moderated.

Conclusion

In the present study, 3D controlled rhBMP-2 delivery systems based on 3D printing technology were successfully developed to enhance segmental bone regeneration without inflammatory response. Sustained and burst releases of rhBMP-2 were realized by dispensing collagen and gelatin gel, respectively, into a PCL/PLGA framework. In the *in vitro* release tests, it was confirmed that rhBMP-2 from the PCL/PLGA/collagen was controllably released for more than a month. In contrast, ~88% of loaded rhBMP-2 from the uncross-linked gelatin gel was released within 24 h. Overall, sustained release of rhBMP-2 from group 3 induced the osteogenic differentiation of hTMSCs *in vitro* and accelerated the new bone formation in the 20-mm rabbit radius defect without significant inflammatory response. On the other hand, the burst release of rhBMP-2 from group 2 did not cause an enhancement of segmental bone regeneration in a rabbit model at week 4 due to the severe inflammatory response provoked by burst release of rhBMP-2. In conclusion, 3D printing-based rhBMP-2-loaded scaffolds with a sustained release rate could be a clinically relevent alternative for segmental bone regeneration in orthopedics.

Acknowledgment

This work was supported by the National Research Foundation of Korea (NRF) grant funded by the Korea Government (MS1P) (No. 2010-0018294 and 2011-0030075).

Disclosure Statement

No competing financial interests exist.

References

1. Burastero, G., Scarfi, S., Ferraris, C., Fresia, C., Sessarego, N., Fruscione, F., Monetti, F., Scarfo, F., Schupbach, P., Podesta, M., Grappiolo, G., and Zocchi, E. The association of human mesenchymal stem cells with BMP-7 improves bone regeneration of critical-size segmental bone defects in athymic rats. Bone **47,** 117, 2010.
2. Reichert, J.C., Saifzadeh, S., Wullschleger, M.E., Epari, D.R., Schutz, M.A., Duda, G.N., Schell, H., van Griensven, M., Redl, H., and Hutmacher, D.W. The challenge of establishing preclinical models for segmental bone defect research. Biomaterials **30,** 2149, 2009.
3. Iacobellis, C., Berizzi, A., and Aldegheri, R. Bone transport using the Ilizarov method: a review of complications in 100 consecutive cases. Strat Traum Limb Recon **5,** 17, 2010.
4. Sen, M.K., and Miclau, T. Autologous iliac crest bone graft: should it still be the gold standard for treating nonunions? Injury **38,** S75, 2007.
5. Deie, M., Ochi, M., Adachi, N., Nishimori, M., and Yokota, K. Artificial bone grafting [calcium hydroxyapatite ceramic with an interconnected porous structure (IP-CHA)] and core decompression for spontaneous osteonecrosis of the femoral condyle in the knee. Knee Surg Sports Traumatol Arthrosc **16,** 753, 2008.
6. Sakurakichi, K., Tsuchiya, H., Kabata, T., Yamashiro, T., Watanabe, K., and Tomita, K. Correction of juxtaarticular deformities in children using the Ilizarov apparatus. J Orthop Sci **10,** 360, 2005.
7. Schaaf, H., Lendeckel, S., Howaldt, H.P., and Streckbein, P. Donor site morbidity after bone harvesting from the anterior iliac crest. Oral Surg Oral Med Oral Pathol Oral Radiol Endod **109,** 52, 2010.
8. Shen, H., Hu, X., Yang, F., Bei, J., and Wang, S. An injectable scaffold: rhBMP-2-loaded poly(lactide-co-glycolide)/hydroxyapatite composite microspheres. Acta Biomater **6,** 455, 2010.
9. Han, L.H., Suri, S., Schmidt, C.E., and Chen, S. Fabrication of three-dimensional scaffolds for heterogeneous tissue engineering. Biomed Microdevices **12,** 721, 2010.
10. Jung, J.W., Kang, H.W., Kang, T.Y., Park, J.H., Park, J., and Cho, D.W. Projection image-generation algorithm for fabrication of a complex structure using projection-based microstereolithography. Int J Precis Eng Man **13,** 445, 2012.
11. Hutmacher, D.W., Sittinger, M., and Risbud, M.V. Scaffold-based tissue engineering: rationale for computer-aided design and solid free-form fabrication systems. Trends Biotechnol **22,** 354, 2004.
12. Seol, Y.J., Kang, T.Y., and Cho, D.W. Solid freeform fabrication technology applied to tissue engineering with various biomaterials. Soft Matter **8,** 1730, 2012.

13. Schuckert, K.H., Jopp, S., and Teoh, S.H. Mandibular defect reconstruction using three-dimensional polycaprolactone scaffold in combination with platelet-rich plasma and recombinant human bone morphogenetic protein-2: *de novo* synthesis of bone in a single case. Tissue Eng Part A **15,** 493, 2009.
14. Peck, J.N., and Marcellin-Little, D.J. Advances in small animal total joint replacement. In: Marcellin-Little, D.J., and Harrysson, O.L.A., eds. Custom Total Joint Arthroplasty. Hoboken, NJ: John Wiley and Sons, Inc., 2013, pp. 223–241.
15. Shor, L., Guceri, S., Chang, R., Gordon, J., Kang, Q., Hartsock, L., An, Y., and Sun, W. Precision extruding deposition (PED) fabrication of polycaprolactone (PCL) scaffolds for bone tissue engineering. Biofabrication **1,** 015003, 2009.
16. Yeo, A., Sju, E., Rai, B., and Teoh, S.H. Customizing the degradation and load-bearing profile of 3D polycaprolactone-tricalcium phosphate scaffolds under enzymatic and hydrolytic conditions. J Biomed Mater Res B **87,** 562, 2008.
17. Li, R.H., and Wozney, J.M. Delivering on the promise of bone morphogenetic proteins. Trends Biotechnol **19,** 255, 2001.
18. Sethi, A., Craig, J., Bartol, S., Chen, W., Jacobson, M., Coe, C., and Vaidya, R. Radiographic and CT evaluation of recombinant human bone morphogenetic protein-2-assisted spinal interbody fusion. Am J Roentgenol **197,** W128, 2011.
19. Wei, S., Cai, X., Huang, J., Xu, F., Liu, X., and Wang, Q. Recombinant human BMP-2 for the treatment of open tibial fractures. Orthopedics **35,** e847, 2012.
20. Lee, J., Decker, J.F., Polimeni, G., Cortella, C.A., Rohrer, M.D., Wozney, J.M., Hall, J., Susin, C., and Wikesjo, U.M. Evaluation of implants coated with rhBMP-2 using two different coating strategies: a critical-size supraalveolar peri-implant defect study in dogs. J Clin Periodontol **37,** 582, 2010.
21. Li, B., Yoshii, T., Hafeman, A.E., Nyman, J.S., Wenke, J.C., and Guelcher, S.A. The effects of rhBMP-2 released from biodegradable polyurethane/microsphere composite scaffolds on new bone formation in rat femora. Biomaterials **30,** 6768, 2009.
22. Vo, T.N., Kasper, F.K., and Mikos, A.G. Strategies for controlled delivery of growth factors and cells for bone regeneration. Adv Drug Deliver Rev **64,** 1292, 2012.
23. Park, J.K., Shim, J.H., Kang, K.S., Yeom, J., Jung, H.S., Kim, J.Y., Lee, K.H., Kim, T.H., Kim, S.Y., Cho, D.W., and Hahn, S.K. Solid free-form fabrication of tissue-engineering scaffolds with a poly(lactic-co-glycolic acid) grafted hyaluronic acid conjugate encapsulating an intact bone morphogenetic protein-2/poly(ethylene glycol) complex. Adv Funct Mater **21,** 2906, 2011.
24. Lee, J.W., Kang, K.S., Lee, S.H., Kim, J.Y., Lee, B.K., and Cho, D.W. Bone regeneration using a microstereolithography-produced customized poly(propylene fumarate)/diethyl fumarate photopolymer 3D scaffold incorporating BMP-2 loaded PLGA microspheres. Biomaterials **32,** 744, 2011.
25. Sawyer, A.A., Song, S.J., Susanto, E., Chuan, P., Lam, C.X., Woodruff, M.A., Hutmacher, D.W., and Cool, S.M. The stimulation of healing within a rat calvarial defect by mPCL-TCP/collagen scaffolds loaded with rhBMP-2. Biomaterials **30,** 2479, 2009.
26. Kim, J.Y., Yoon, J.J., Park, E.K., Kim, D.S., Kim, S.Y., and Cho, D.W. Cell adhesion and proliferation evaluation of SFF-based biodegradable scaffolds fabricated using a multi-head deposition system. Biofabrication **1,** 015002, 2009.
27. Kim, J.Y., and Cho, D.W. Blended PCL/PLGA scaffold fabrication using multi-head deposition system. Microelectron Eng **86,** 1447, 2009.
28. Hwang, S.H., Kim, S.Y., Park, S.H., Choi, M.Y., Kang, H.W., Seol, Y.J., Park, J.H., Cho, D.W., Hong, O.K., Rha, J.G., and Kim, S.W. Human inferior turbinate: an alternative tissue source of multipotent mesenchymal stromal cells. Otolaryngol Head Neck Surg **147,** 568, 2012.
29. Hwang, S.H., Kim, S.W., Kim, S.Y., Park, S.H., Lee, H.J., Choi, M.Y., Oh, H.J., Kim, S.H., Rhie, J.W., and Sun, D.I. Human turbinate mesenchymal stromal cells as a potential option for cartilage tissue engineering. Tissue Eng Regen Med **8,** 536, 2011.
30. Hwang, S.H., Kim, S.Y., Park, S.H., Choi, M.Y., Back, S.A., Kim, Y.I., Sun, D.I., and Kim, S.W. Osteogenic differentiation of human turbinate mesenchymal stromal cells. Tissue Eng Regen Med **8,** 544, 2011.
31. Shim, J.H., Kim, J.Y., Park, M., Park, J., and Cho, D.W. Development of a hybrid scaffold with synthetic biomaterials and hydrogel using solid freeform fabrication technology. Biofabrication **3,** 034102, 2011.
32. Shim, J.H., Kim, J.Y., Park, J.K., Hahn, S.K., Rhie, J.W., Kang, S.W., Lee, S.H., and Cho, D.W. Effect of thermal degradation of SFF-based PLGA scaffolds fabricated using a multi-head deposition system followed by change of cell growth rate. J Biomat Sci Polym E **21,** 1069, 2010.
33. Kim, J.Y., Jin, G.Z., Park, I.S., Kim, J.N., Chun, S.Y., Park, E.K., Kim, S.Y., Yoo, J., Kim, S.H., Rhie, J.W., and Cho, D.W. Evaluation of solid free-form fabrication-based scaffolds seeded with osteoblasts and human umbilical vein endothelial cells for use *in vivo* osteogenesis. Tissue Eng Part A **16,** 2229, 2011.
34. Shields, L.B., Raque, G.H., Glassman, S.D., Campbell, M., Vitaz, T., Harpring, J., and Shields, C.B. Adverse effects associated with high-dose recombinant human bone morphogenetic protein-2 use in anterior cervical spine fusion. Spine **31,** 542, 2006.
35. Friess, W., Uludag, H., Foskett, S., Biron, R., and Sargeant, C. Characterization of absorbable collagen sponges as rhBMP-2 carriers. Int J Pharm **187,** 91, 1999.
36. Kirker-Head, C.A. Potential applications and delivery strategies for bone morphogenetic proteins. Adv Drug Deliver Rev **43,** 65, 2000.
37. Abarrategi, A., Civantos, A., Ramos, V., Sanz Casado, J.V., and Lopez-Lacomba, J.L. Chitosan film as rhBMP2 carrier: delivery properties for bone tissue application. Biomacromolecules **9,** 711, 2008.
38. Uludag, H., D'Augusta, D., Palmer, R., Timony, G., and Wozney, J. Characterization of rhBMP-2 pharmacokinetics implanted with biomaterial carriers in the rat ectopic model. J Biomed Mater Res **46,** 193, 1999.
39. Zhou, H., Qian, J., Wang, J., Yao, W., Liu, C., Chen, J., and Cao, X. Enhanced bioactivity of bone morphogenetic protein-2 with low dose of 2-N, 6-O-sulfated chitosan *in vitro* and *in vivo*. Biomaterials **30,** 1715, 2009.
40. Jeon, O., Song, S.J., Yang, H.S., Bhang, S.H., Kang, S.W., Sung, M.A., Lee, J.H., and Kim, B.S. Long-term delivery enhances *in vivo* osteogenic efficacy of bone morphogenetic protein-2 compared to short-term delivery. Biochem Biophys Res Commun **369,** 774, 2008.
41. Maegawa, N., Kawamura, K., Hirose, M., Yajima, H., Takakura, Y., and Ohgushi, H. Enhancement of osteo-

blastic differentiation of mesenchymal stromal cells cultured by selective combination of bone morphogenetic protein-2 (BMP-2) and fibroblast growth factor-2 (FGF-2). J Tissue Eng Regen Med **1,** 306, 2007.
42. Ma, P.X. Biomimetic materials for tissue engineering. Adv Drug Deliver Rev **60,** 184, 2008.
43. Itoh, S., Nakamura, S., Kobayashi, T., Shinomiya, K., Yamashita, K., and Itoh, S. Effect of electrical polarization of hydroxyapatite ceramics on new bone formation. Calcified Tissue Int **78,** 133, 2006.
44. Schlichting, K., Schell, H., Kleemann, R.U., Schill, A., Weiler, A., Duda, G.N., and Epari, D.R. Influence of scaffold stiffness on subchondral bone and subsequent cartilage regeneration in an ovine model of osteochondral defect healing. Am J Sports Med **36,** 2379, 2008.
45. Hutmacher, D.W. Scaffolds in tissue engineering bone and cartilage. Biomaterials **21,** 2529, 2000.
46. Van den Berg, T.K., and Kraal, G. A function for the macrophage F4/80 molecule in tolerance induction. Trends Immunol **26,** 506, 2005.
47. Julka, A., Shah, A.S., and Miller, B.S. Inflammatory response to recombinant human bone morphogenetic protein-2 use in the treatment of a proximal humeral fracture: a case report. J Shoulder Elb Surg **21,** e12, 2012.
48. Lacey, D.C., Simmons, P.J., Graves, S.E., and Hamilton, J.A. Proinflammatory cytokines inhibit osteogenic differentiation from stem cells: implications for bone repair during inflammation. Osteoarthritis Cartilage **17,** 735, 2009.
49. Mountziaris, P.M., and Mikos, A.G. Modulation of the inflammatory response for enhanced bone tissue regeneration. Tissue Eng Part B **14,** 179, 2008.

Address correspondence to:
Dong-Woo Cho, PhD
Department of Mechanical Engineering
Pohang University of Science and Technology (POSTECH)
San 31, Hyoja-dong, Nam-gu, Pohang
Kyungbuk 790-784
South Korea

E-mail: dwcho@postech.ac.kr

Seong Soo Kang, DVM, PhD
Department of Surgery
College of Veterinary Medicine
Chonnam National University
Gwangju 500 757
South Korea

E-mail: vetkang@chonnam.ac.kr

Received: August 16, 2013
Accepted: January 27, 2014
Online Publication Date: March 14, 2014